Available online at www.sciencedirect.com
SCIENCE DIRECT®
Synthetic Metals 141 (2004) 113–122
SYNTHETIC METALS
www.elsevier.com/locate/synmet

Functionalization of carbon nanotubes

H. Kuzmany [a,*], A. Kukovecz [b], F. Simon [a], M. Holzweber [a], Ch. Kramberger [a], T. Pichler [c]

[a] *Institute for Materials Physics, University of Vienna, Strudlhofgasse 4, A-1090 Vienna, Austria*
[b] *Department of Applied and Environmental Chemistry, University of Szeged, Rerrich B. 1, H-6720 Szeged, Hungary*
[c] *Leibnitz Institut für Festkörper- und Werkstofforschung, Dresden, Germany*

Received 11 July 2003; accepted 19 August 2003

Abstract

The functionalization of single wall carbon nanotubes (SWCNTs) is a very actively discussed topic in contemporary nanotube literature because the planned modification of SWCNT properties is believed to open the road towards real nanotechnology applications. In this contribution, some recent results are reported on the subject. Covalent attachment of functional groups, their influence on tube-tube stacking, detachment of functional groups, selective n- and p-type intercalation as well as special reactions carried out in the interior of SWCNTs are discussed. Clean room conditions for interior of single wall carbon nanotubes is demonstrated.

Keywords: Carbon; Nanotubes; Vibrations; Raman; Functionalization

1. Introduction

As a consequence of their unusual physical properties and large application potential, single wall carbon nanotubes (SWCNTs) have attracted the interest of scientists and engineers ever since their discovery in 1993 [1]. This interest was dramatically raised with the discovery of routes to grow them in high yield [2]. The small diameter of the tubes leads to macroscopic quantization of the electronic and vibrational states in transversal direction and to a reduced dimensionality along the tube axis. Formally derived from the graphene sheet they exhibit unusual mechanical properties such as high toughness and high elastic moduli. Referring to their electronic structure, they exhibit semiconducting as well as metallic behavior and thus cover the full range of properties important for technology [3]. Applications in compound materials, electronic devices, nanosensors or as gas storage material are intensively explored. All these potential applications require an extended functionalization of the nanotubes to make them processable and to tune their properties.

One disadvantage of all carbon nanotubes is their insolubility in any solvent. Only suspensions of the tubes can be produced. Solubility is an urgent property for processability even as far as it concerns purification. Functionalization by chemical reactions with extended molecular chains—similarly as it is now well understood for fullerenes—should help. Functionalization of this type creates a new class of materials with new properties, again in direct analogy to functionalized fullerenes. Functionalization may as well help to separate semiconducting tubes from metallic ones, to purify nanotubes from carbonaceous impurities or to reduce the width of diameter dispersion. Alternative ways to functionalize carbon nanotubes are by substitution reactions such as replacement of carbon atoms from the tube wall by boron or nitrogen [4]. In principle functionalization should also be possible from the inside of the tubes. On this topic good progress has been obtained recently from experiments to study chemical reactions inside the nanotubes [5]. The physics and chemistry of this concave nanospace bears a big challenge for material science. Unexpected new materials were already grown and more are on their way. The properties of these new compounds have to be explored.

Graphite and similarly graphene are well known to be chemically highly inert structures. Like in fullerenes reactivity is activated by curvature effects. Curvature in nanotubes is much smaller than in conventional fullerenes: firstly since the tube diameters are generally larger and secondly since they are curved in one direction only. One way to increase reactivity is therefore to study tubes with smaller diameters. Even though such tubes become eventually unstable due to their high curvature energy they are of basic interest. Not only do they exhibit enhanced chemical reactivity but also show enhanced deviation from the planar graphene

* Corresponding author. Tel.: +43-1-4277-51306; fax: +43-1-4277-51357.
E-mail address: kuzman@ap.univie.ac.at (H. Kuzmany).

0379-6779/$ – see front matter © 2003 Elsevier B.V. All rights reserved.
doi:10.1016/j.synthmet.2003.08.018

properties. Very narrow tubes were even demonstrated to exhibit superconducting fluctuations up to 15 K.

In this paper, we present some recent results on the chemical functionalization of SWCNT and on chemical reactions and reaction products in the curved nanospace inside the tubes. These reports are preceded by a compilation of SWCNT materials and experimental and analytical procedures used for their study. With respect to the latter particular attention is paid to resonance Raman scattering.

2. Single wall carbon nanotubes

Single wall carbon nanotubes can be understood as rolled up stripes of graphene sheets. Each lattice vector of the sheet determines a particular nanotube by rolling up the sheet in a way that the origin and the top of the lattice vector come to coincidence. This generating vector is called Hamada-vector or folding vector (n, m). Along the tube axis lattice periodicity is provided and the size of the unit cell, including the tube diameter, is determined by the Hamada-vector of the tube. The geometry is depicted in Fig. 1. As long as the carbon–carbon distances are assumed independent from the rolling up process the tube diameter d and the number of carbon atoms per unit cell N can be read directly from the figure as

$$d = \frac{a}{\pi}\sqrt{n^2 + m^2 + nm} \tag{1}$$

$$N = \frac{2(m^2 + n^2 + nm)}{d_R} \tag{2}$$

where $a = 2.41$ Å is the lattice constant of the unrolled honeycomb lattice and d_R is defined as

$$d_R = \begin{cases} d_H & \text{if } (n-m) \text{ is not a multiple of } 3d_H \\ 3d_H & \text{if } (n-m) \text{ is a multiple of } 3d_H \end{cases} \tag{3}$$

where d_H denotes the highest common divisor of n and m.

For small tube diameters Eq. (1) is not valid any more and ab initio density functional calculations are needed to obtain

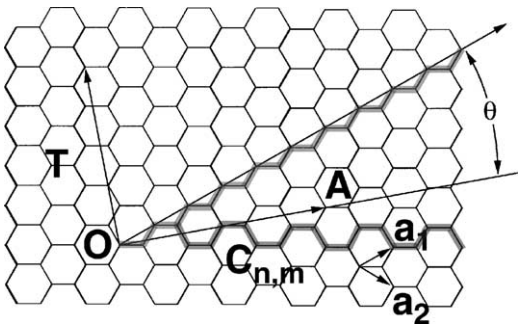

Fig. 1. Basics of SWCNT geometry. Lattice vectors are denoted $\boldsymbol{a}_1$ and $\boldsymbol{a}_2$, while the OA vector is the $\boldsymbol{C}$ chiral vector of the (4, 2) tube. The two gray contour lines indicate the cross-sections of the two limiting cases of graphene sheet folding: the zigzag (n, 0) and the armchair (n, n) nanotubes, respectively. The θ angle is the chiral angle of the nanotube.

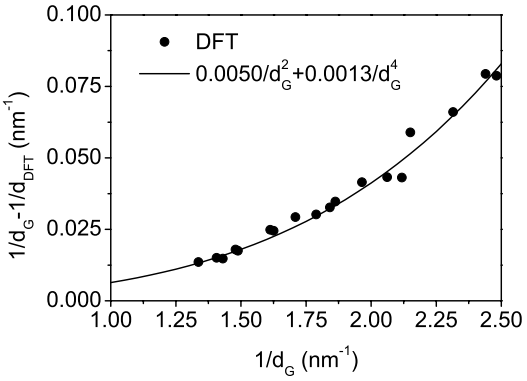

Fig. 2. Difference between inverse tube diameters calculated from density functional theory and zone folding for small tubes vs. inverse zone folding diameters.

the correct tube geometry. Fortunately, the reduced number of carbon atoms in the small tubes allows for such calculations at least up to (5, 6) or $d = 0.75$ nm. Fig. 2 depicts results we have obtained recently from such calculations. For the spectroscopic analysis of small tubes the deviations from the graphene geometry cannot be neglected.

Several SWCNT synthesis methods are available today (see Table 1 for a survey). In general, SWCNTs always grow from carbon plasma in the presence of structure directing agents. The latter are usually in situ formed transition metal (Co, Fe, Ni, V, etc.) nanoparticles, although in special cases (peapod to DWCNT conversion, CNT growth within zeolites) steric limitations can also provide the necessary structure directing constraints. The most important differences between the available methods are (i) the way the plasma is generated, (ii) the way the catalyst metal is introduced, (iii) SWCNT yield, (iv) SWCNT quality and (v) possibilities of up-scaling and commercialization. While at present the majority of the world's SWCNT production comes from the two conventional sources (PLV and dc arc), it is expected that continuous and less power-hungry methods (gas phase decomposition and CCVD) will eventually become the major industrial SWCNT suppliers. The CCVD method is unique since it is the only technique that makes precise spatial SWCNT positioning possible.

One of the classical methods to analyze SWCNT is transmission electron microscopy (TEM). Even though this technique provides direct evidence for some geometrical properties of the tubes it is very site selective and does not give representative results. On the other hand Raman spectroscopy, in particular with its characteristic resonance enhancement, has proven to be an excellent analytical tool [13]. Two spectral ranges are particularly useful for analytical purposes: the range of the radial breathing mode (RBM) between 150 and 450 cm^{-1} and the so called D-line between 1250 and 1400 cm^{-1}.

The RBM is a typical feature of the nanotubes as it does not exist in the graphene plane. Since the mode frequency scales as $1/d$, where d is the tube diameter, it can be used

Table 1
A summary of the contemporary SWCNT synthesis techniques and product description

Short name	Technology of preparation [reference]	Typical mean diameter (nm)	Product description
Laser ablation (PLV)	Ablation from graphite doped with (Fe, Co, Ni, ...) catalyst [2]	1.4 (1–1.8)	High quality, good diameter control, bundled tubes; commercial
dc arc discharge	First reported production. Modified Kratschmer reactor [6]	1.5 (0.9–3.1)	Lesser quality, carbonaceous impurities abundant. CNTs grow bundled
Gas phase decomposition	Decomposition in an oxygen-free environment. Typical: HiPco® (high pressure CO decomposition) [7]	1 (0.9–1.3)	Easy purification, commercial, good quality
CCVD	Catalytic chemical vapor deposition. Supported metal catalysts are used [8]	1.5 (1.3–2)	Cheapest, commercial, up-scalable. Most feasible from the application point of view
Flame pyrolysis	Carbon source + metallocene catalyst, conventional low pressure pyrolysis reactor [9]	2–3	Low yield, bad quality. Still under development. Plant technology available, large commercialization potential
Solar furnace	Solar rays focused on a metal doped graphite target. Growth dynamics similar to PLV [10]	1.4	Good quality CNTs, little amorphous carbon. Spreading not expected in the near future
Inner tubes of DWCNTs	Catalyst free growth from peapods by coalescence of C_{60} molecules [11]	0.7 (0.55–1)	Well shielded, best quality CNTs. Separation from outer tubes is very challenging
Zeolite grown	CNTs grow by thermal decomposition of template molecules within zeolite channels [12]	0.45	Monodisperse diameter distribution, oriented tubes. CNTs metastable outside the channels

to determine tube diameters in principle. Unfortunately, the scaling factor is not known with a high precision. Reported values are between 23 and 48 cm^{-1} [14–16] which allows only an order of magnitude evaluation for absolute values or the evaluation of relative tube diameters and tube diameter distributions [13]. An additional difficulty in the assignment of Raman lines to tube diameters is the high density of geometrically allowed tubes of the order of 15 tubes per nanometer diameter difference or accordingly one tube per wave number difference. This holds at least for standard tube diameters. The resulting overlap of Raman lines is lifted for very small tube diameters as it is demonstrated below. For such tubes the overlap problem is not relevant but now the 1/d law is not well satisfied and ab initio density functional calculations (DFT) are needed to evaluate the tube diameters. On the other hand, as the energy gap between the van Hove singularities in the valance band and in the conduction band also scales with the inverse tube diameter, photoselective resonance scattering is observed [17] and leads to a colorful response in Raman experiments if the spectra are excited with different laser energies [18].

The D-line response is the other important analytical tool. From some very recent work its origin is well understood as a response from the K-point of the graphene Brillouin zone with an enhancement from a triple resonance scattering [19,20]. The scattering process needs an impurity or a defect to be involved for momentum conservation. Therefore the scattering cross section of the D-line depends on the defect concentration and can be used as a measure of the latter. An attractive quantity for this concentration is the relative scattering intensity of the D-line and its overtone, the so called G′ line. The G′ line is also triple resonance enhanced but independent from any defect concentration.

NMR spectroscopy, as such certainly a qualified tool to study functionalization, turned out to be less efficient for long time due to magnetic contamination from catalytic particles. Such particles are difficult to remove since they are often covered up with a carbon layer. Similarly, IR spectroscopy did not provide a good access to SWCNT analysis. However, in the case of chemical functionalization the side groups respond in general well to IR absorption.

Raman spectra recorded in this contribution were obtained on a triple grating Dilor xy spectrometer utilizing a back-thinned CCD detector. Samples for the Raman measurements were in buckypaper form. FT-IR spectra were recorded on a Bruker IFS-66v instrument in reflection absorption geometry.

3. Exohedral chemical functionalization of SWCNTs

The perfect SWCNT is without functional groups and therefore chemically quite inert. Addition-based covalent chemistry on nanotubes is more difficult than transforming fullerenes but is considerably easier than functionalizing graphite. The two main sources of reactivity in SWCNTs are (i) the curvature-induced strain arising from the non-planar geometry of sp^2 carbons and (ii) the misalignment of the π orbitals [21]. The former is more pronounced (i.e. the pyramidalization angle is larger) at the capping fullerene

hemispheres while the latter effects mainly the side-walls. All in all, the most reactive places in any nanotube sample are found in the cap of the thinnest tube and least reactive are the bonds running perpendicular to the axis of the largest diameter SWCNT.

Derivatization reactions can be roughly divided into two categories. In the first case, the required functional groups are attached directly onto the nanotube using 1,3-dipolar cycloaddition [22], the Birch reduction [23] and reactions with nitrenes, radicals and carbenes [24]. When taking the second approach we first build bridgeheads by oxidizing some atoms in the tube wall and then proceed using substitution reactions to change the simple (–F, –OH, –COOH) groups formed. The first reaction step is usually some aggressive treatment, e.g. (i) oxidation in refluxing conc. HNO_3 (yields carboxyl groups) [25–27], (ii) ozone treatment [28,29], (iii) ball milling in reactive atmosphere [30] or together with solid KOH (hydroxyl groups) [31], (iv) HF reaction (–F groups) [32,33]. Then in the second step these bridgeheads are converted to more reactive groups, e.g. carboxyl groups are replaced by acyl chlorides after $SOCl_2$ treatment and finally, conventional organic synthesis reactions like the Grignard reaction [34] are applied to build the desired functionality onto the anchor sp^3 carbon in the nanotube wall.

In the course of the work reported here first the simplest functionalized SWCNTs were studied: nanotubes with –COOH groups formed upon purification treatment in refluxing HNO_3 [35] (see Fig. 3A for a schematic representation of the material). The presence of the carboxyl groups was proved by FT-IR measurements and earlier ^{13}C NMR investigations. In Fig. 4, we present the resonance Raman spectra of the pristine and the functionalized nanotube sample in the RBM region for three selected laser excitation energies. It is interesting to note that the RBM suffers an approx. 8 cm^{-1} up-shift upon functionalization without changing its shape. This phenomenon cannot be explained on the basis of resonant Raman theory alone. Instead, we interpret it as a token of increased stacking interaction within the SWCNT bundles. By analyzing the first and second spectral moments of the RBMs we were able to quantify the extent of this interaction and suggest that the SWCNT bundles after oxidative functionalization contain 6–10 times more nanotubes than before. A possible reason for this behavior could be that the formed carboxyl groups favor the development of intertube H-bonds.

Advancing towards more complex functional groups we investigated the properties of SWCNTs functionalized with the 1,3-dipolar cycloaddition reaction of azomethine yields (see Fig. 3B) [22]. The attachment of the sidechain is evident from the FT-IR spectrum of the material (Fig. 5A) where e.g. the contributions of the ν(N–H), ν(C–H) and ν_{as}(C–O–C) vibrations can be clearly identified at around 3400, 3000 and 1100 cm^{-1}, respectively. In agreement with independent literature reports we have also found the functionalized SWCNT material to be luminescent which prevented direct resonance Raman investigations. The special importance of this functionalization scheme is that the resulting nanotubes become soluble in organic solvents (up to 50 mg/ml in $CHCl_3$) and even in water. Dissolved nanotubes can be separated from impurities by e.g. chromatographic techniques and finally, the original SWCNT structure can be restored by thermal annealing [36]. In Fig. 5B, we present the Raman RBM spectra of the nanotubes before functionalization and after annealing. It is evident from the figure that the RBM modes characteristic for SWCNT samples are recovered by heating.

As demonstrated above, functionalization can affect the constitution of SWCNT bundles when the attached functional groups act as stacking modifiers. Curiously enough, the reverse statement also proved to be valid: the intertube channels are indeed able to affect the functionality of nanotubes by acting as size-selective filters allowing doping species to enter certain bundles and stay clear from others (Fig. 3C) [37]. Fig. 6 depicts present Raman spectra of HiPco® SWCNTs in various stages of potassium intercalation (n-type doping). It can be seen that the RBM lines corresponding to the thinnest and thickest nanotubes are selectively reduced, whereas the modes originating from intermediate tube diameters are not effected that much. Since the diameter of the intertube channels is maximal in the bundles of the thickest nanotubes, the selective reduction of the low wavenumber RBM peaks can be explained simply by geometrical constraints. While not that straightforward, the interpretation of the loss of the peaks corresponding to the thinnest SWCNTs is also possible by realizing that the lattice expansion work required for the potassium dopant to enter the bundle is the smallest in the case of the smallest tube diameters [38]. Very similar trends could be observed in a parallel set of experiments utilizing $FeCl_3$ dopant (p-type doping). The electronic properties of SWCNTs are heavily influenced by both n- and p-type doping. Therefore, the described diameter dependent doping phenomenon may find important applications in nanotube functionalization, especially when high selectivity is required.

4. The concave nanospace inside the tubes as a chemical reactor

4.1. Filling SWCNT with fullerenes

The inside of carbon cages is certainly interesting from a chemical point of view as the distribution of the carbon π orbitals is quite different in comparison to their distribution on the outside. Fig. 7 gives a demonstration for a (7, 7) tube. The smaller the tube diameter the more deviation is established form a clean π–π overlap.

Experimentally very little is known about the interior of carbon cages. The reason is the fact that so far all attempts failed to open the fullerene cages and to inspect the interior chemically by studying reactions in the concave environment of the carbon atoms. Experimentalists were

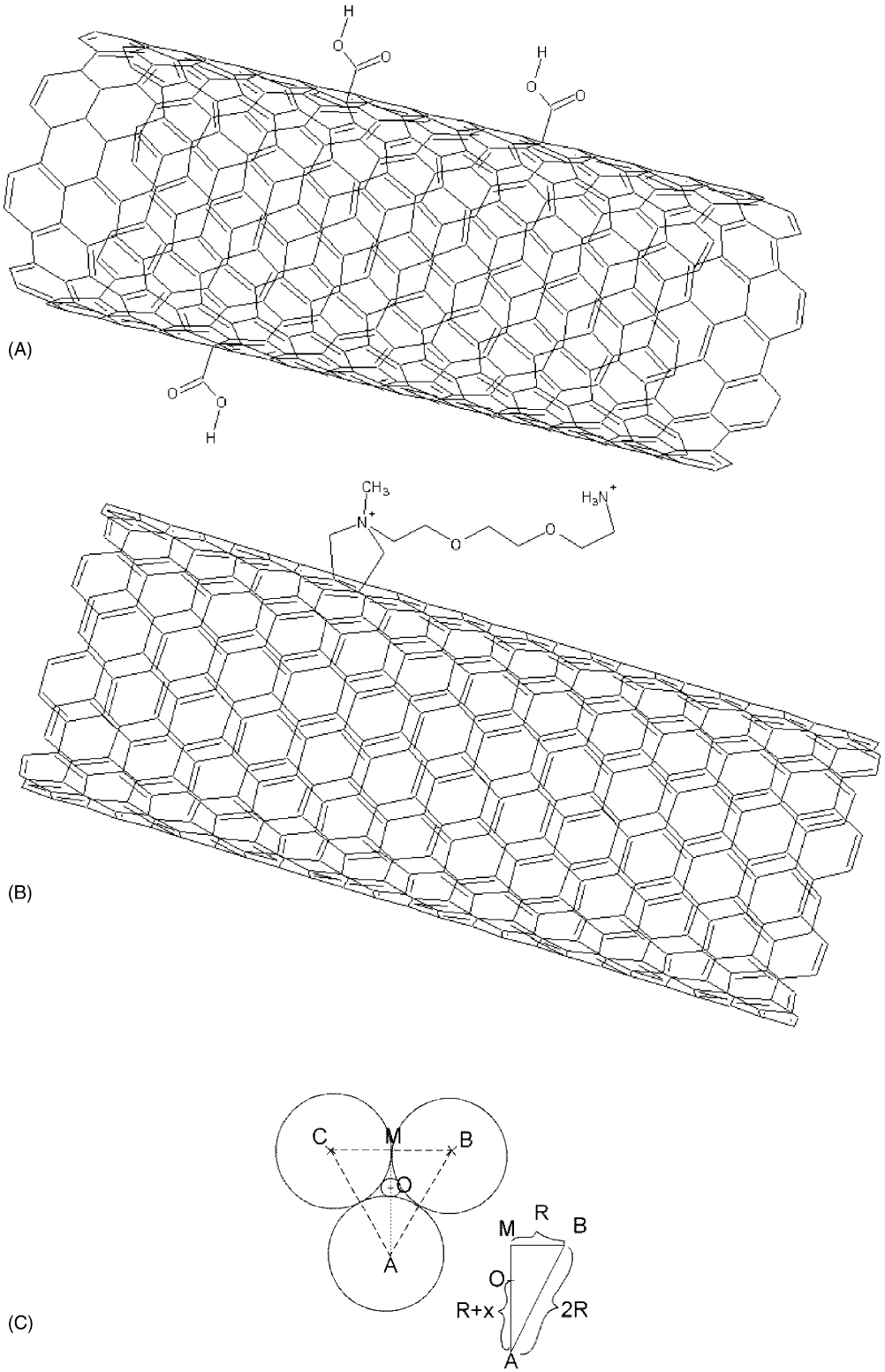

Fig. 3. Visualization of the functionalized SWCNT material studied here: (A) carboxy-functionalized nanotube, (B) solubilized nanotube, (C) basics of calculating the x radius of the intertube channels in a triangular lattice containing r_{NT} radius tubes that have an additional r_{vdW} van der Waals radius around them. $R = r_{NT} + r_{vdW}$. The sides of the ABC triangle are equal, therefore, the O point divides the MA segment in a 1:2 ratio.

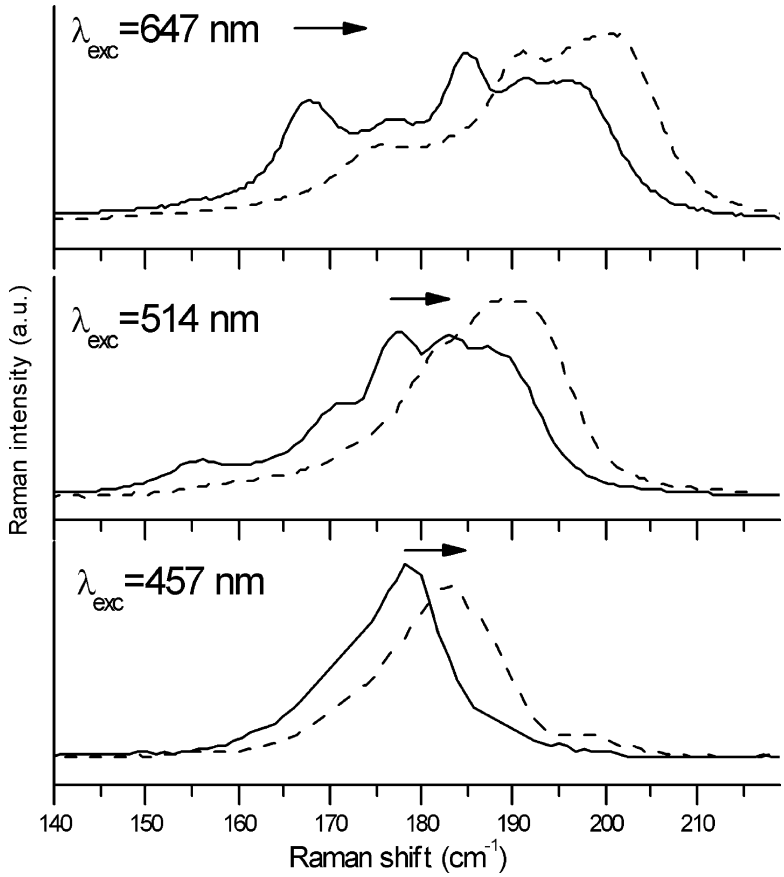

Fig. 4. Resonant Raman spectra of pristine (solid line) and carboxy functionalized (dashed line) SWCNT material in the radial breathing mode region, measured with three different laser lines.

left with the cumbersome purification procedure of material where atoms were incidentally encaged during the growth process. Considerable progress was made recently at this point by discovering a possibility to fill the nanotubes with fullerenes [39] or, more generally, with matter [40]. Particular interest was directed to the filling of single wall carbon nanotubes with C_{60} fullerenes in order to make so called "peapods".

In our experiments commercial SWCNT (Nanocarblab, Moscow, Russia) and fullerenes ('super golden grade' Hoechst AG, Frankfurt, Germany) were used for the production of fullerene peapods. The SWCNT material was prepared by dc arc-discharge and was purified to 50% using repeated high temperature air and acid washing treatments by the manufacturer. Purity was determined from HR-TEM by the supplier and it is consistent with our own studies. The high filling levels discussed below are consistent with the effective tube-end opening side-effect of the SWCNT purification [41]. We found that the other reported tube-end opening procedure, i.e. refluxing in H_2O_2 [42], does not increase the fullerene filling levels. We followed the method of Kataura et al. [42] to fill fullerenes in the vapor phase. This method involves sealing of the SWCNT material with the fullerene in a quartz ampoule and keeping it at 650 °C for 2 h. The resulting material was thoroughly sonicated in toluene in order to remove the non-reacted fullerenes, filtered, and dried from toluene at 400 °C in dynamic vacuum. A 30 min dynamic vacuum treatment at 800 °C is equivalent to this last step in removing non-reacted fullerene particles without observable effect on the peapods.

Both TEM and Raman scattering are excellent tools to analyze the filling of SWCNTs with fullerenes. Fig. 8 is an example for SWCNTs filled with C_{60} (A) and C_{70} (B). As already mentioned above, due to the site selectivity of the TEM technique it is difficult to determine filling concentrations from such experiments. In the Raman response the scattering from the nanotube modes as well as the scattering from the enclosed fullerenes appears [5,42]. In the case of C_{60} a characteristic splitting pattern of the total symmetric modes, the pentagonal pinch mode and the radial breathing mode, is a reliable signature for the C_{60} cages encapsulated into the tubes [43]. The relative intensities of these modes to the RBM mode and to the G mode of the tubes is a quantitative measure for the filling concentration [44]. Absolute values of the filling concentration can be obtained from electron energy loss spectra (EELS) [45]. Results from EELS and Raman are in good agreement and provide therefore reliable numbers for the filling.

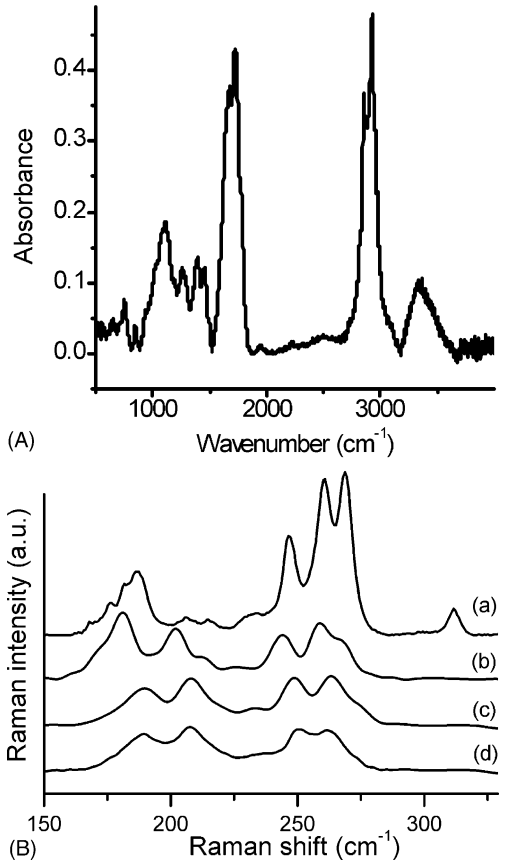

Fig. 5. Spectroscopic study on the solubilized SWCNTs: (A) FT-IR spectrum of the material, (B) resonant Raman spectra of the pristine (a), annealed pristine (b), functionalized and heated (c) and functionalized, heated and annealed (d) SWCNT samples.

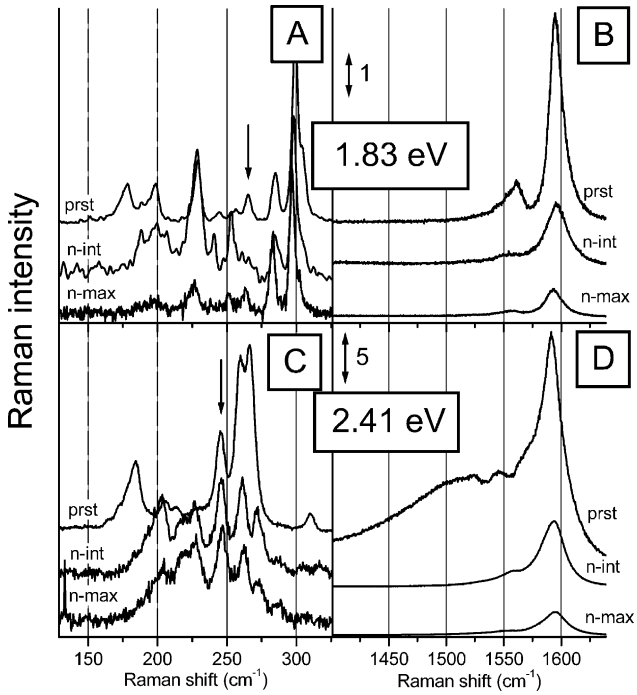

Fig. 6. Development of Raman spectra during the K (n-type) doping of the HiPco® sample. Top row: 1.83 eV excitation. Bottom row: 2.41 eV excitation. Plots (A and C) and (B and D) show the RBM and the G line windows, respectively. In all plots, "prst" marks the spectrum of undoped tubes while "n-int" and "n-max" denote the intermediate and the final stages of the doping process. To make a comparison between relative peak intensities easier, the 1.83 and 2.41 eV RBM spectra are normalized to the intensity of the 265 and 245 cm^{-1} peak, respectively. These peaks are indicated by vertical arrows in the plots. For the G-lines, intensities within one plot are measured on the same scale which is given in the top left corner [38]. Reproduced by permission of the PCCP Owner Societies.

4.2. Polymerization of fullerenes inside the SWCNT

We studied recently two types of chemical reactions of the encaged peas in the nanotubes. One of them is a polymerization of C_{60} fullerenes after heavy doping of the peapod system with electron donors such as alkali metals [5,46]. The results of the doping process on the Raman response are demonstrated in Fig. 9 for potassium doping. The shift of the pentagonal pinch mode of the encapsulated C_{60} as demonstrated in the figure is about 40 cm^{-1}. This means 6 extra electrons are accommodated on the fullerene cage. The results become even more interesting if the response from the radial modes of the C_{60} is analyzed. This response is depicted in Fig. 10 in comparison with the response from C_{60}^{6-} in a crystal and from a typical polymeric phase of C_{60}. The strong features assigned as P at 360 and 620 cm^{-1} are typical signatures from a polymeric phase. These lines have been observed several times in neutral and doped C_{60} polymers. Though slightly shifted they are well pronounced in the selected example of RbC_{60}. A polymeric phase of K_6C_{60} has not been observed so far for C_{60} outside the tubes. From calculation of reaction enthalpies reported by Pekker et al. [47], a linear single bonded C_{60}^{6-} polymeric phase is the second most stable polymeric structure in the system of charged C_{60} molecules. It is thus very likely that the charged C_{60}^{6-} cages have reacted to this structure in the tubes.

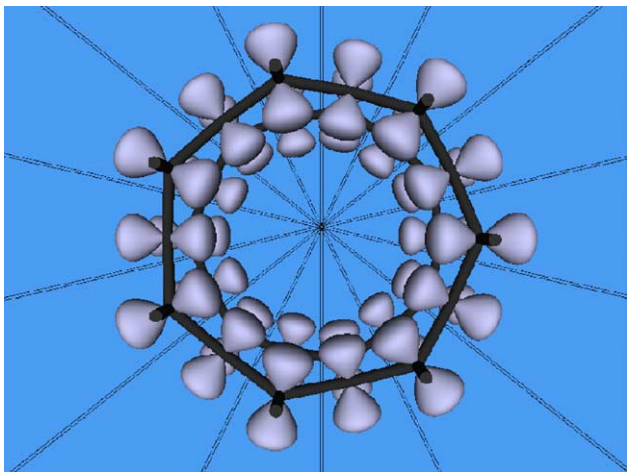

Fig. 7. Schematic view of electronic orbitals inside a (7, 7) single wall carbon nanotube.

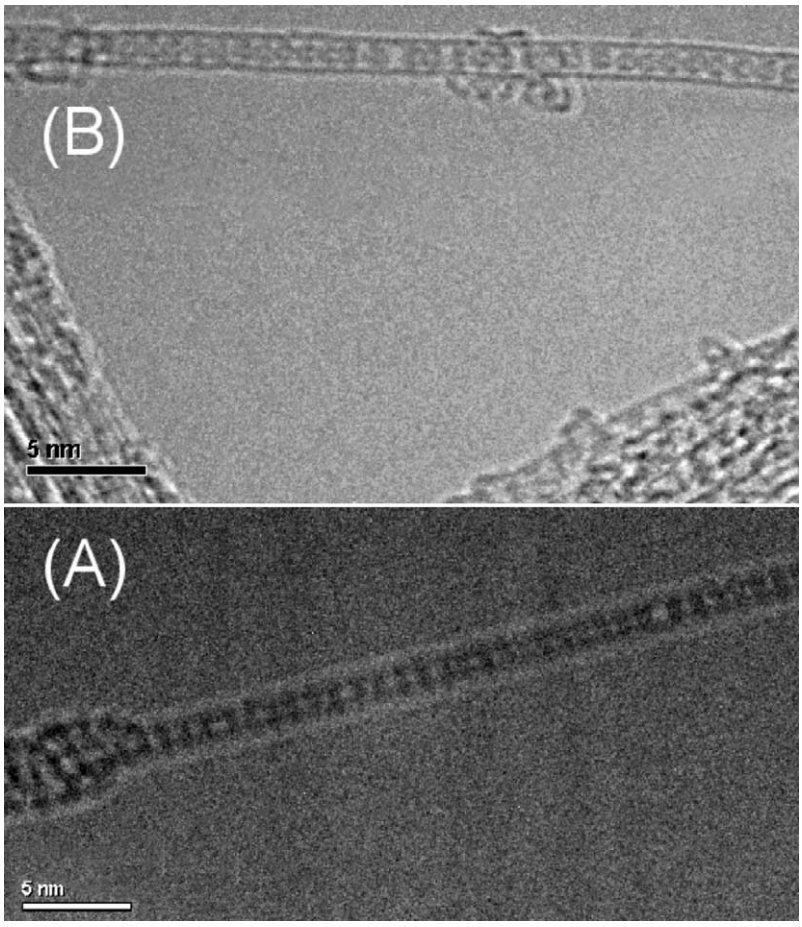

Fig. 8. Transmission electron micrographs of individual tubes filled with C_{60} (A) and C_{70} (B).

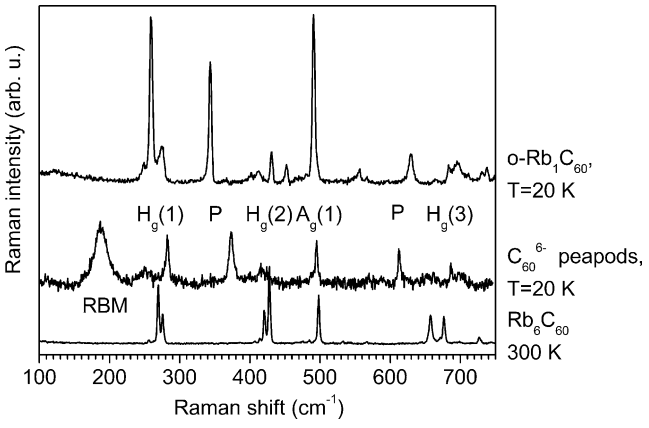

Fig. 9. Raman response of the tangential mode frequency range for potassium doped SWCNTs and potassium doped peapods. Spectra were excited with three different lasers as indicated. The first, third, and fifth spectrum from the bottom are for empty tubes, the second forth and sixth spectrum are for filled tubes. The right arrow assigns the frequency of the pentagonal pinch mode for the uncharged C_{60}, the left arrow marks the frequency after long doping.

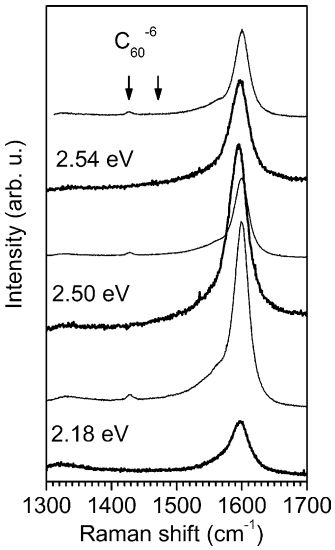

Fig. 10. Raman spectra of the radial part of charged C_{60} as recorded with a green laser line at 514 nm and temperatures as indicated. The spectra at the bottom, in the center, and at the top are for crystalline C_{60}^{6-}, for the heavily doped peapods, and for an one-dimensional polymeric phase of C_{60}^{-}, respectively.

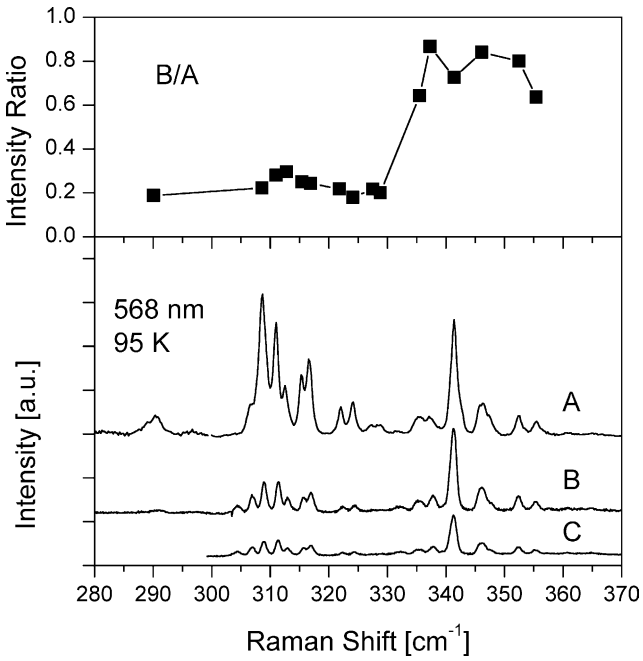

Fig. 11. Growth of DWCNTs from peapods by vacuum annealing at 1520 K. The lower part depicts thee spectra: (C) after 30 min annealing, (B) after 60 min annealing, and (A) after 120 min (saturation) annealing. The upper part depicts the relative intensities of the Raman lines in spectrum B to spectrum (A).

4.3. Generation of double wall carbon nanotubes

The other reaction inside the tube which we have recently investigated is a transformation of the encaged fullerenes to a second inner tube forming the double wall carbon nanotube (DWCNT) system. The creation of DWCNT from the encapsulated fullerene peas was first demonstrated by Bandow et al. by a TEM analysis of high temperature treated peapods [11]. For the growth process several models were proposed. Either the fullerene cages connect via a cyclo-addition process and subsequent Stone-Wales reactions transform the connected cages eventually to an inner tube [48] or the cages break up into small pieces, like e.g. C_2 units, and recondense as an inside tube. Fig. 11 depicts Raman spectra of the radial breathing mode of the inner shell tubes after extended annealing at 1520 K in high vacuum. We demonstrated recently that each (split) peak in the spectrum corresponds to one tube species [49]. The high frequency lines originate from the small tubes with diameters below 0.7 nm. For short annealing times mainly the peas in the narrow tubes transform to the inner shell tube. Only for extended annealing the larger diameter tubes follow. This is explicitly demonstrated in the top part of the figure which exhibits the intensity ratio between the lines in spectrum B to the lines in spectrum A. This result disfavors the cyclo-addition and Stone–Wales transformation model since in the latter high mobility of the peas is requested. Such high mobility is rather provided by the large tubes. The cyclo addition model is also disfavored from our observation that encaged C_{60} and encaged C_{70} molecules give almost the same line pattern after annealing. In other words the same kind of inner tubes are created even though the larger size of the C_{70} molecules does not allow room for a cyclo addition reaction if the tube size is too small for an upright ordering of the elongated C_{70} molecule.

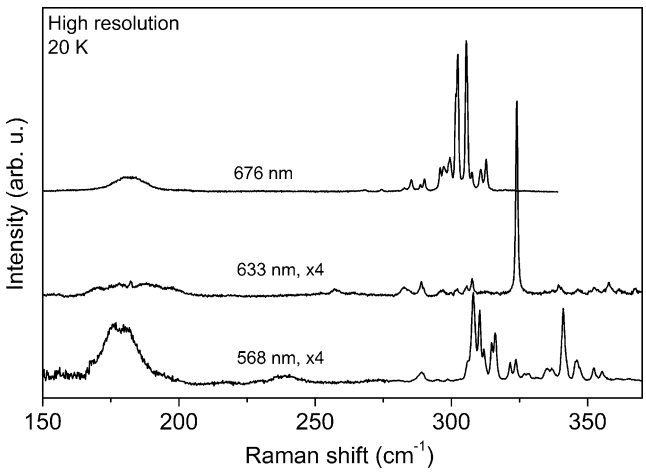

Fig. 12. Raman response of RBMs from outer shell and inner shell tubes in DWCNTs prepared from C_{60} at SWCNT peapods. Inner shell tubes give 10 times higher peaks.

The structural properties of the inner shell tubes in the DWCNT system are interesting by themselves. The widths of the Raman lines from the inner shell RBM response is unusual narrow, of the order of 0.5 cm^{-1} but extends down to even lower values. This means the interior of the primary, outer tubes is highly shielded and the inner tubes exhibit a high degree of perfectness. They are catalyst free grown in a “nano cleanroom”. An example for the narrow lines is depicted for three different excitation energies in Fig. 12. The broad lines on the left side represent the response from the outer shell tubes, the narrow lines on the right come from the inner shell. Also, particularly for the excitation with the deep red laser, the peak and total intensities for the scattering from the inner tubes are almost a factor of 10 higher than the scattering from the outer tubes. Very sharp resonances and an enhanced electron-phonon coupling is likely to be the reason for this dramatic behavior. The enhanced electron-phonon coupling for strong curvature carbon surfaces is not unexpected as calculations for small fullerenes have repeatedly demonstrated such effects [50].

5. Summary

The reported results demonstrate that various ways exist to functionalize SWCNT. Functional groups covalently attached to the outer surface of the nanotubes are able to modify the stacking and solvatation properties of nanotubes. An interesting feature of SWCNT bundles is that their n- and p-type intercalation proceeds in a diameter dependent way, thus making it in principle possible to selectively modify

certain nanotubes while leaving others intact. Functionalization inside the tubes in the form of covalent chemical bonds has not yet been demonstrated but chemical reactions which lead to products not observed outside the tubes occur. Such reactions are the polymerization of charged fullerene cages and the catalyst free growth of SWCNTs with a high degree of perfectness. The fullerenes in the smaller tubes exhibit a higher probability for the transformation process as compared to the fullerenes in the larger tubes.

Acknowledgements

The authors acknowledge financial support from the EU RTN FUNCARS (HPRN-CT-1999-00011) and FWF Austria project No. 14386. Valuable discussions with Prof. M. Prato and V. Georgakilas from the University of Trieste are also gratefully acknowledged. A.K. thanks for a support from a Zoltan Magyary fellowship. All authors thank J. Bernardi for the assistance with the TEM studies.

References

[1] S. Iijima, T. Ichihashi, Nature 363 (1993) 603.
[2] T. Guo, P. Nikolaev, A. Thess, D.T. Colbert, R.E. Smalley, Chem. Phys. Lett. 243 (1995) 49.
[3] M.S. Dresselhaus, G. Dresselhaus, P.C. Eklund, Science of Fullerenes and Carbon Nanotubes, Academic Press, San Diego, 1996.
[4] D. Golberg, Y. Bando, W. Han, K. Kurashima, T. Sato, Chem. Phys. Lett. 308 (1999) 337.
[5] T. Pichler, H. Kuzmany, H. Kataura, Y. Achiba, Phys. Rev. Lett. 8726 (2001).
[6] S. Iijima, Nature 354 (1991) 56.
[7] P. Nikolaev, M.J. Bronikowski, R.K. Bradley, F. Rohmund, D.T. Colbert, K.A. Smith, R.E. Smalley, Chem. Phys. Lett. 313 (1999) 91.
[8] J.F. Colomer, C. Stephan, S. Lefrant, G. Van Tendeloo, I. Willems, Z. Konya, A. Fonseca, C. Laurent, J.B. Nagy, Chem. Phys. Lett. 317 (2000) 83.
[9] R.L. Vander Wal, T.M. Ticich, V.E. Curtis, J. Phys. Chem. A 104 (2000) 7209.
[10] D. Laplaze, P. Bernier, W.K. Maser, G. Flamant, T. Guillard, A. Loiseau, Carbon 36 (1998) 685.
[11] S. Bandow, M. Takizawa, K. Hirahara, M. Yudasaka, S. Iijima, Chem. Phys. Lett. 337 (2001) 48.
[12] Z.K. Tang, H.D. Sun, J. Wang, J. Chen, G. Li, Appl. Phys. Lett. 73 (1998) 2287.
[13] H. Kuzmany, W. Plank, M. Hulman, C. Kramberger, A. Grüneis, T. Pichler, H. Peterlik, H. Kataura, Y. Achiba, Eur. Phys. J. B 22 (2001) 307.
[14] S. Bandow, S. Asaka, Y. Saito, A.M. Rao, L. Grigorian, E. Richter, P.C. Eklund, Phys. Rev. Lett. 80 (1998) 3779.
[15] J. Kürti, G. Kresse, H. Kuzmany, Phys. Rev. B 58 (1998) R8869.
[16] A. Jorio, R. Saito, J.H. Hafner, C.M. Lieber, M. Hunter, T. McClure, G. Dresselhaus, M.S. Dresselhaus, Phys. Rev. Lett. 86 (2001) 1118.
[17] A.M. Rao, E. Richter, S. Bandow, B. Chase, P.C. Eklund, K.A. Williams, S. Fang, K.R. Subbaswamy, M. Menon, A. Thess, R.E. Smalley, G. Dresselhaus, M.S. Dresselhaus, Science 275 (1997) 187.
[18] M. Milnera, J. Kurti, M. Hulman, H. Kuzmany, Phys. Rev. Lett. 84 (2000) 1324.
[19] C. Thomsen, S. Reich, Phys. Rev. Lett. 85 (2000) 5214.
[20] V. Zolyomi, J. Kürti, A. Grüneis, H. Kuzmany, Phys. Rev. Lett. 90 (2003) 157401.
[21] S. Niyogi, M.A. Hamon, H. Hu, B. Zhao, P. Bhowmik, R. Sen, M.E. Itkis, R.C. Haddon, Acc. Chem. Res. 35 (2002) 1105.
[22] V. Georgakilas, K. Kordatos, M. Prato, D.M. Guldi, M. Holzinger, A. Hirsch, J. Am. Chem. Soc. 124 (2002) 760.
[23] S. Pekker, J.P. Salvetat, E. Jakab, J.M. Bonard, L. Forro, J. Phys. Chem. B 105 (2001) 7938.
[24] M. Holzinger, O. Vostrowsky, A. Hirsch, F. Hennrich, M. Kappes, R. Weiss, F. Jellen, Angew. Chem. Int. Ed. 40 (2001) 4002.
[25] C.N.R. Rao, A. Govindaraj, B.C. Satishkumar, Chem. Commun. (1996) 1525.
[26] A. Kuznetsova, I. Popova, J.T. Yates, M.J. Bronikowski, C.B. Huffman, J. Liu, R.E. Smalley, H.H. Hwu, J.G.G. Chen, J. Am. Chem. Soc. 123 (2001) 10699.
[27] Z.H. Yu, L.E. Brus, J. Phys. Chem. A 104 (2000) 10995.
[28] D.B. Mawhinney, V. Naumenko, A. Kuznetsova, J.T. Yates, J. Liu, R.E. Smalley, J. Am. Chem. Soc. 122 (2000) 2383.
[29] L.T. Cai, J.L. Bahr, Y.X. Yao, J.M. Tour, Chem. Mater. 14 (2002) 4235.
[30] Z. Konya, I. Vesselenyi, K. Niesz, A. Kukovecz, A. Demortier, A. Fonseca, J. Delhalle, Z. Mekhalif, J.B. Nagy, A.A. Koos, Z. Osvath, A. Kocsonya, L.P. Biro, I. Kiricsi, Chem. Phys. Lett. 360 (2002) 429.
[31] H.L. Pan, L.Q. Liu, Z.X. Guo, L.M. Dai, F.S. Zhang, D.B. Zhu, R. Czerw, D.L. Carroll, Nano Lett. 3 (2003) 29.
[32] E.T. Mickelson, C.B. Huffman, A.G. Rinzler, R.E. Smalley, R.H. Hauge, J.L. Margrave, Chem. Phys. Lett. 296 (1998) 188.
[33] K.F. Kelly, I.W. Chiang, E.T. Mickelson, R.H. Hauge, J.L. Margrave, X. Wang, G.E. Scuseria, C. Radloff, N.J. Halas, Chem. Phys. Lett. 313 (1999) 445.
[34] P.J. Boul, J. Liu, E.T. Mickelson, C.B. Huffman, L.M. Ericson, I.W. Chiang, K.A. Smith, D.T. Colbert, R.H. Hauge, J.L. Margrave, R.E. Smalley, Chem. Phys. Lett. 310 (1999) 367.
[35] A. Kukovecz, C. Kramberger, M. Holzinger, H. Kuzmany, J. Schalko, M. Mannsberger, A. Hirsch, J. Phys. Chem. B 106 (2002) 6374.
[36] V. Georgakilas, D. Voulgaris, E. Vazquez, M. Prato, D.M. Guldi, A. Kukovecz, H. Kuzmany, J. Am. Chem. Soc. 124 (2002) 14318.
[37] A. Kukovecz, T. Pichler, R. Pfeiffer, H. Kuzmany, Chem. Commun. (2002) 1730.
[38] A. Kukovecz, T. Pichler, R. Pfeiffer, C. Kramberger, H. Kuzmany, PCCP Phys. Chem. Chem. Phys. 5 (2003) 582.
[39] B.W. Smith, M. Monthioux, D.E. Luzzi, Nature 396 (1998) 323.
[40] A. Chu, J. Cook, R.J.R. Heesom, J.L. Hutchison, M.L.H. Green, J. Sloan, Chem. Mater. 8 (1996) 2751.
[41] K. Hirahara, S. Bandow, K. Suenaga, H. Kato, T. Okazaki, H. Shinohara, S. Iijima, Phys. Rev. B 6411 (2001) 115420.
[42] H. Kataura, Y. Maniwa, T. Kodama, K. Kikuchi, K. Hirahara, K. Suenaga, S. Iijima, S. Suzuki, Y. Achiba, W. Kratschmer, Synth. Met. 121 (2001) 1195.
[43] R. Pfeiffer, 2003, in press.
[44] H. Kuzmany, R. Pfeiffer, C. Kramberger, T. Pichler, X. Liu, M. Knupfer, J. Fink, H. Kataura, Y. Achiba, B.W. Smith, D.E. Luzzi, Appl. Phys. A: Mater. Sci. Process 76 (2003) 449.
[45] X. Liu, T. Pichler, A. Knupfer, M.S. Golden, J. Fink, H. Kataura, Y. Achiba, K. Hirahara, S. Iijima, Phys. Rev. B 6504 (2002) 045411.
[46] T. Pichler, A. Kukovecz, H. Kuzmany, H. Kataura, Y. Achiba, Phys. Rev. B 67 (2003).
[47] S. Pekker, G. Oszlanyi, G. Faigel, Chem. Phys. Lett. 282 (1998) 435.
[48] D. Tomanek, Personal communication, 2003.
[49] R. Pfeiffer, H. Kuzmany, C. Kramberger, C. Schaman, T. Pichler, H. Kataura, Y. Achiba, J. Kurti, V. Zolyomi, Phys. Rev. Lett. 90 (2003) 225501.
[50] N. Breda, R.A. Broglia, G. Colo, G. Onida, D. Provasi, E. Vigezzi, Phys. Rev. B 62 (2000) 130.